Acoustic Characterization of the NASA Langley 14- by 22-Foot Subsonic Tunnel Using Single-Microphone Analysis Techniques

Colin M. Stutz[1], Mary L. Houston, Nikolas S. Zawodny, Kyle A. Pascioni
NASA Langley Research Center
2 N. Dryden Steet, Hampton, VA

ABSTRACT

An experimental campaign was conducted to assess recent acoustic modifications to the NASA Langley Research Center 14- by 22-Foot Subsonic Tunnel. This effort was undertaken in preparation for future rotorcraft, Advanced Air Mobility, and airframe noise acoustic tests. The tunnel is a closed circuit and typically operates in an open-jet configuration for acoustic studies. A vertical linear array of microphones and a phased array were placed on traverses outside of the core flow. Pole-mounted acoustic sources with known waveforms were used to identify reflective surfaces under static conditions with no tunnel flow. A similar process was replicated with more compact sources in an aerodynamic fairing for flow speeds up to Mach 0.16. This enabled investigation of the test section core flow and bounding shear layer impacts on the acoustic measurements. Periodic averaging was employed and was shown to be capable of isolating periodic acoustic signals even for poor signal-to-noise ratio conditions. Benefits and limitations of single-microphone processing methods are identified. A companion paper utilizes a phased array in an effort to address the identified limitations to more traditional single-microphone data collection.

1. INTRODUCTION

There is an ever-present desire to conduct experimental research at larger scales while maintaining a controlled environment. This is especially true to aeroacoustics research, where directly relating results from scaled tests to full-scale vehicles can be difficult. These considerations make larger-scale facilities like the NASA Langley's 14- by 22-Foot Subsonic Tunnel (commonly referred to as the 14x22) a valuable asset. Recent aeroacoustic entries in the 14x22 have included scaled models of the full-span NASA Hybrid Wing Body [1], a semi span Gulfstream aircraft [2], and a semispan High-Lift Common Research Model [3, 4]. These tests were largely focused on scaled airframe noise and propulsion airframe aeroacoustics, which for the tested scales are high-frequency acoustic

[1]colin.m.stutz@nasa.gov

phenomena on the order of $O(10^3)$ - $O(10^5)$ Hz. Work has been done to improve the acoustic treatment in the 14x22 test section since the completion of these tests. One of the driving factors for the treatment improvements has been a desire to return to scaled rotorcraft-type tests in the 14x22, where the tonal acoustic content is often on the order of $O(10^2)$ Hz. A rotor-focused acoustics test has not been performed in the 14x22 in roughly 30 years [5]. The background noise of the 14x22 in its acoustic configuration was characterized as part of the Hybrid Wing Body test [6], however, the flow speed range of that characterization (Mach 0.11 to 0.23) and subsequent modifications to the treatment necessitates facility re-characterization.

To that end, an experimental campaign to characterize the 14x22 for acoustic testing was completed. New floor treatment, which will be documented in greater detail in a forthcoming publication [7], was deployed for the test, and measurements in the empty test section with and without flow were performed. Measurements were collected with microphones in a linear array and a phased array, the latter of which will be discussed in a companion paper (Houston et al., *Noise-Con* 2024 [8]). These characterizations included identifying major acoustic reflection surfaces in the empty test section and background noise levels with and without flow. Known noise sources were used in this test, which allowed for the application of processing methods such as periodic averaging and the rejection of hydrodynamic pressure fluctuations.

2. EXPERIMENTAL SETUP AND METHODS

This test was conducted in the NASA Langley Research Center 14- by 22-Foot Subsonic Tunnel. The 14x22 is a closed-circuit atmospheric tunnel that can be operated in closed- and open-jet configurations. The test section is 14.5 ft (4.42 m) tall, 21.75 ft (6.63 m) wide, and 50 ft (15.24 m) long. The walls and ceiling are lifted out of the test section to achieve the open-jet configuration, leaving the floor in place, as shown in Figure 1. In this sense, the 14x22's "open-jet" configuration is better characterized as a quasi-open-jet. A collector at the downstream end of the test section is used to capture the expanded shear layer and direct the flow into the tunnel circuit. The open-jet configuration is typically used for acoustic tests in this tunnel, as was the case in this work. The tunnel can operate between Mach numbers of 0.02 and 0.26 in the open-jet configuration, however this test focused on Mach numbers of 0.16 and below. Flow speeds for this test were determined via a Pitot-static probe located at the inlet of the test section.

A schematic of the full tunnel circuit can be found in Manuel et al. [9], however the focus of Manuel et al. was to redesign the flow collector, so the schematic is not representative of the current installed flow collector. Figure 1 includes an image of the test section set up for this test (looking upstream) as well as a basic model of the test section that will be discussed in further detail in Section 3.1. The north wall of the test section (to the left, if looking upstream from the collector) is treated with 6-in melamine foam wedges, which have a nominal cut-on frequency of 500 Hz. The ceiling, after being raised for the open-jet configuration, is also acoustically treated with the same wedges as the north wall. The south wall (to the right, if looking upstream from the collector) is treated with acoustic paneling, consisting of fiber-cloth-wrapped fiberglass covered by perforated metal panels. Two floor carts make up 50 ft (25 ft each) of the floor in the streamwise direction, starting roughly 1 foot from the inlet of the test section (beneath and supporting the baskets, which are the bright white floor section in Figure 1). These carts were lowered 2 ft to allow for the placement of

acoustic treatment in "baskets". The baskets used in this test were a new iteration on the existing facility design, using two densities of foam, 2 lb/ft^3 and 6 lb/ft^3, as fill material. The fill material was constrained on the sides by a coarse wire mesh. The top of the baskets had two components. Directly on top of the foam was a rigid wire grid of 1/4-in diameter and 3-in by 3-in cells. An 1/8-in thick felt sheet (with an area density of 18 oz/yd^2) was stretched over the grid and fastened to the wire mesh on the sides of the baskets to minimize scrubbing noise. A previous iteration of the baskets used an adhesive-backed felt laid over the baskets, however, subsequent work showed that the adhesive backing was acoustically hard [7]. Six-in thick cloth-covered fiberglass was installed on the floor in a wooden frame in the area between the baskets and the north and south walls to reduce floor reflections outside of the core flow. Six-in thick polyurethane foam was used for the two downstream-most panels to avoid interactions between the cloth covering and the expanded shear layer. Previous tests used 4-in thick polyurethane foam glued to the floor to acoustically treat the out-of-flow floor area. The previous floor treatment was disposed of at the end of each test, whereas the new treatment can be re-used in future entries.

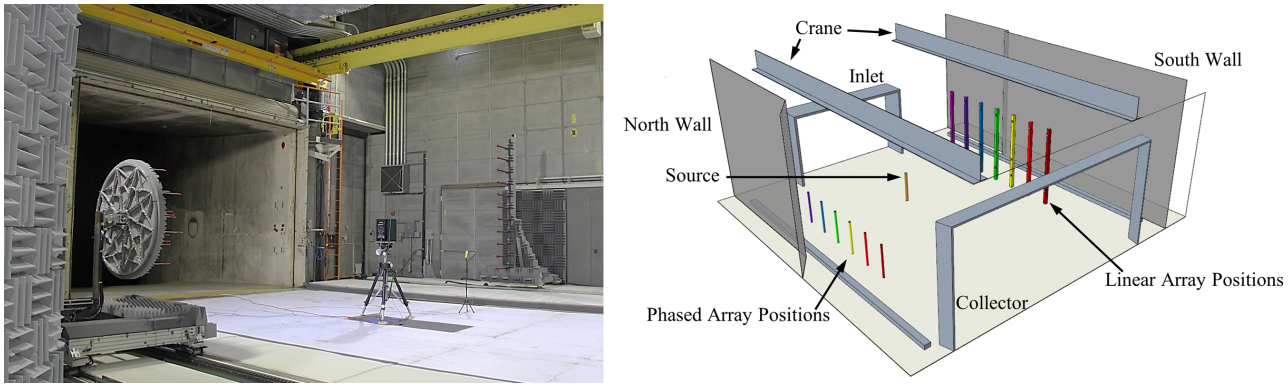

Figure 1: Image (left) and rudimentary model (right) of the 14x22 test section. *Image credit: NASA*

Multiple acoustic sources were leveraged in this study and can be broadly categorized as "static" sources, used with no flow in the tunnel, and "in-flow" sources, which were used with flow in the test section. All of the acoustic sources were positioned 16 ft (4.88 m) downstream of the inlet, 5 ft above the floor, and nominally centered laterally in the test section. The static sources were placed on tripods and the in-flow sources were housed in a custom fairing mounted to an aerodynamic strut with a 16-in chord NACA 0024 profile.

Two static sources were used in this test. A Mackie® HR824 cabinet speaker, which is a directional speaker with a nominally flat output across the frequency range of interest of 100 Hz to 20 kHz, and a NTI Audio DS3 Dodecahedron omnidirectional speaker were used. The directional speaker provided the ability to focus on possible reflective surfaces in front of and behind the microphones, such as the floor, walls, and microphone mounting hardware, whereas the omnidirectional speaker aided in identifying reflections from surfaces such as the inlet and collector of the test section, and surfaces farther upstream and downstream in the tunnel circuit. There were also two in-flow sources used. The first was a small directional speaker with a Dayton DMS58 2-in driver. Compared with the Mackie speaker, this speaker had a lower maximum output frequency but was significantly smaller, which allowed it to be placed in an aerodynamic fairing. A second directional source, a pneumatic "airball", was then used to target the higher frequency range with a random white noise signal for the cases with freestream flow. The airball consisted of an aluminum hemisphere with an array of

pinholes that generated high-frequency random broadband noise when pressurized air was passed through it. Samples of each acoustic source generating a broadband white noise waveform are shown in Figure 2. A bandpass filter was applied to the collected data, with corner frequencies selected such that there was less than 0.1 dB attenuation over the specified frequency range of each waveform. The background data sets, which had no generated waveform, were bandpassed from 50 Hz to 100 kHz.

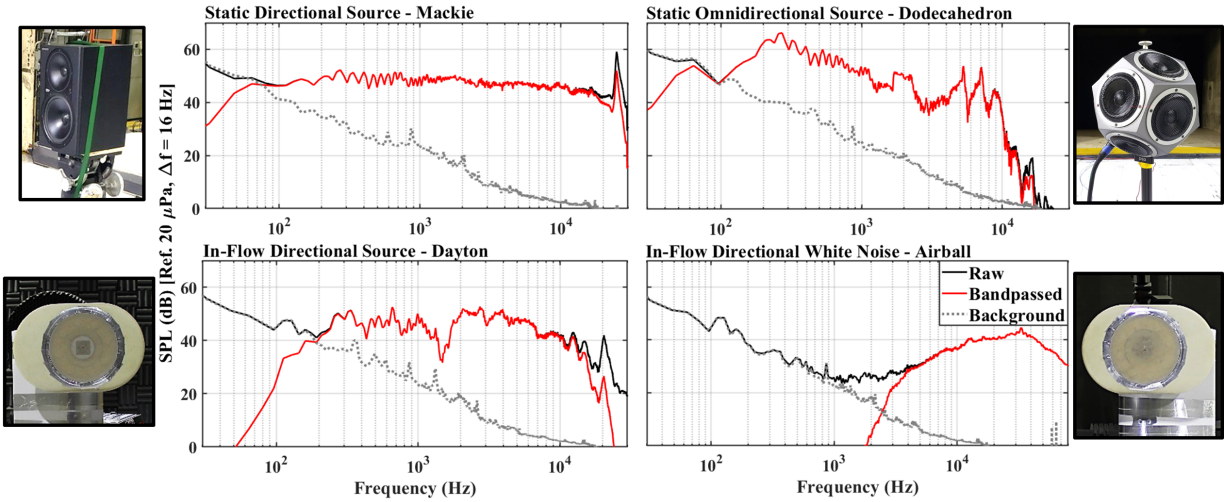

Figure 2: Samples of broadband noise waveforms from each source without flow. Note different frequency range for the airball source. *Image credit: NASA*

Multiple waveforms were used for the speaker outputs, all 60 seconds long. Random white noise signals were generated with bounds between 100 Hz and 20 kHz, with the 60-second signal being repeatable. A periodic "multisine" signal was also generated [10], with the same frequency bounds as the white noise and a period of 0.5 seconds. This signal allowed for the use of periodic averaging on broadband signals. Another set of waveforms included impulses with peak frequencies of 2.5, 5, 10, and 20 kHz, also repeated at 0.5-second intervals. These were used to isolate acoustic reflections. The last set of waveforms was pure tones that were generated at the one-third octave band center frequencies up to 16 kHz. The pure-tone signals were reduced to a duration of 30 seconds.

Two microphone arrays were deployed simultaneously for this test. Both arrays were mounted on automated linear stages outside of the core flow, allowing them to be traversed in the streamwise direction. Five streamwise positions were investigated, from 8 ft upstream of the source to 8 ft downstream of the source, in 4-ft intervals. Data presented in this work will be from the center position, streamwise co-located with the acoustic source, unless specified otherwise. A phased array was mounted on the traverse on the north side of the test section, 187 in from the tunnel centerline. The design, performance, and results from the phased array are discussed in a companion paper (Houston et al., *Noise-Con* 2024 [8]). The second array consisted of 11 Brüel & Kjær Type 4939 1/4-in microphones arranged on a vertical linear tower, as shown in Figure 3. The microphones were spaced 1 ft apart, with the lowest microphone 28 in from the floor (22 in from the top of the out-of-flow treatment). This placed microphone 8 close to the same height as the center of the acoustic sources. The tower was constructed using 80-20 rail with diagonal supports in the streamwise (downstream side) and streamnormal (behind) directions. The rail was treated with 8-in foam wedges, which have a nominal cut-on frequency of 400 Hz, to reduce reflections. The microphones were mounted at the end of 3-ft long aluminum tubes, which were wrapped in foam.

This placed the microphones 194 in from the tunnel centerline. Data were sampled from the linear array microphones at 204,800 samples per second, which was selected to ensure resolvable frequency content up to 80 kHz. The microphones were fitted with wind screens to isolate them from any potential hydrodynamic pressure fluctuations from the shear layer and to protect the exposed diaphragms. The wind screens used a double layer of nylon stockings stretched over a frame made of two bent 0.050-in diameter nitinol rods.

3. RESULTS AND DISCUSSION

3.1. Test Section Reflection Identification

The first effort of the test was to identify the potential reflective surfaces of the test section. A rudimentary computer model of the test section was therefore created to aid in the identification of the sources of the strong reflections by determining propagation paths and times for surface reflections. Measurements for the model were collected with tape measures and often across rather large distances, so the dimensions are not highly accurate, however, they were considered sufficient for this effort. Figure 1 shows the computer model, with all five different streamwise positions of the arrays. The center of the phased array and source are captured in the model, along with the positions of microphones 1, 8, and 11 in the linear array (top, nearest to acoustic source, and bottom, respectively).

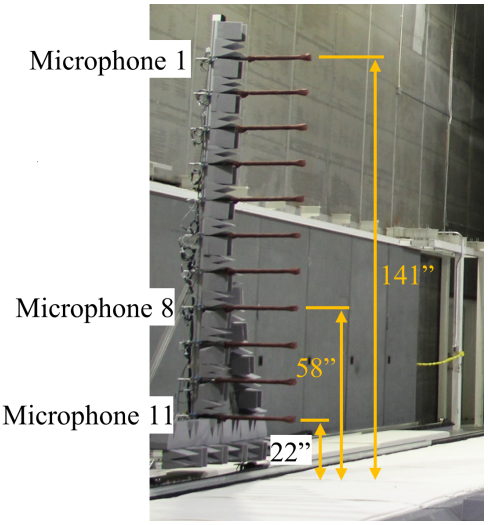

Figure 3: Linear tower array, as viewed from upstream. *Image credit: NASA*

The reflective surfaces that were identified as potentially the most significant were the floor, the walls, the collector, the crane rails, and the upstream and downstream corners in the tunnel circuit. Figure 4 demonstrates identifying the strongest of the potential reflective surfaces using an impulse centered at 2.5 kHz from the dodecahedron. The value of the impulse waveforms is also demonstrated in this figure. Periodically averaging the pressure time history, i.e., ensemble-averaging blocks with a period equal to that of the repeating waveform, reduces the prominence of random components and provides a clear visualization of the pressure peaks that are indicative of reflections. In a reflection-free facility, only the initial impulse would be present. The periodic-averaging process is discussed in more detail in Section 3.2. Peaks in the pressure data can be observed in Figure 4 at propagation times that are well-aligned with the south wall (which is behind the linear array), both crane rails, and the collector, with the strongest reflections being the south wall and south crane rail. There is also a strong reflection from the floor, but the scaling of the figure obscures that reflection. It appears that there may be a reflection from the upstream corner of the tunnel circuit, however, the figure is not conclusive. Interestingly, there does not appear to be an obvious strong reflection from the opposite (north) wall of the test section. This may be due to the obstructions caused by the source itself and the phased array, or the wedge treatment on the north wall.

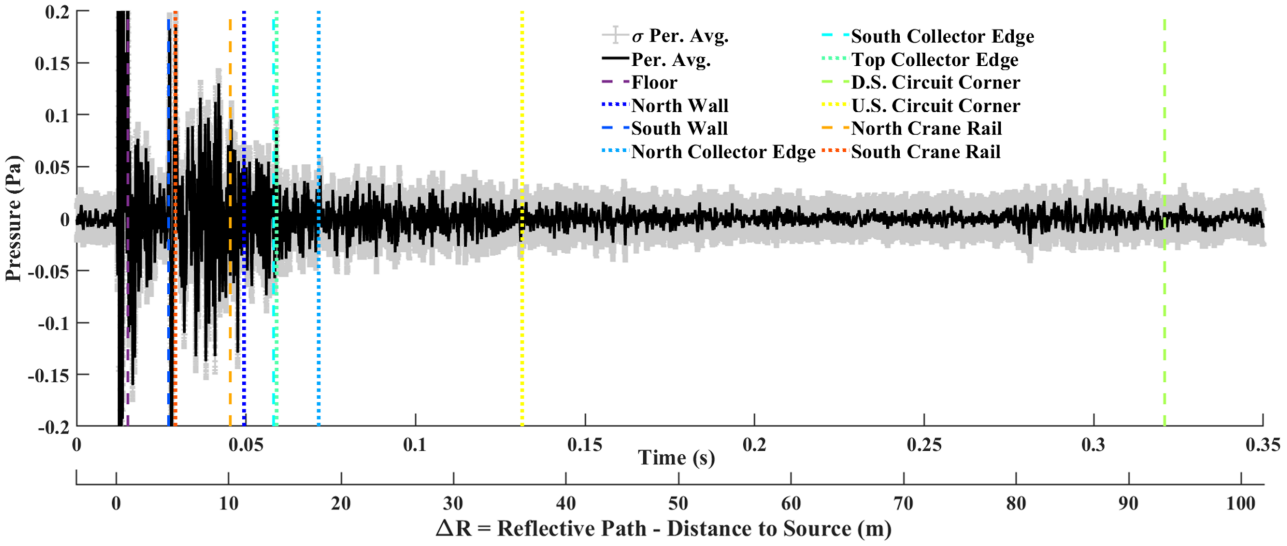

Figure 4: Identification of major reflections for microphone 8 with an impulse signal from the dodecahedron.

Figure 5 focuses on the three strongest reflections, which are the floor, south wall, and south crane, and demonstrates the effect of different streamwise array positions using the omnidirectional dodecahedron source. Note that the floor and south crane reflection times show the symmetry of the streamwise positions of the microphone array with respect to the source. The reflection propagation times for the south wall are not symmetric due to differences in the distance of the wall from the source. A step in the south wall is created by additional panels in the test section that cover observation windows, which can be seen between the fourth and fifth downstream positions of the tower (green and yellow towers) array in Figure 1. Lines marking the reflection propagation times for the tower structure and the ring holding the wind screens are not included in Figure 5, however, those times correlate to the strong reflections that occur between the source impulse and the floor reflections. Similar trends about tunnel reflectivity were observed in the static data from the phased array, however reflections from the north wall (behind the phased array) were dependent on the streamwise position of the phased array. This was due to the asymmetry in the test section, which can be seen in Figure 1.

3.2. Use of Periodic Averaging with Single-Microphone Data

Periodic (or phase) averaging is a method of data processing that leverages consistently repeating content in a signal to improve the quality of measured signals and remove stochastic background noise. This is a valuable tool in rotorcraft acoustics, where certain tones are generated by the rotation of the blades at predictable periods [11–14]. Periodically repeating waveforms, as identified in Section 2, were leveraged to investigate the use of periodic averaging in future 14x22 rotorcraft tests. These waveforms repeated twice per second for a total of 60 seconds, providing at least 118 cycles of the full signal. The recorded pressure data were then divided into 0.5-second intervals and the intervals were averaged to create a single 0.5-second representation of the waveform. Figure 6 shows the averaged pressure signal for the periodic multisine waveform at a set of freestream Mach numbers. Note that these signals were generated using the fairing-mounted Dayton speaker as the in-flow source.

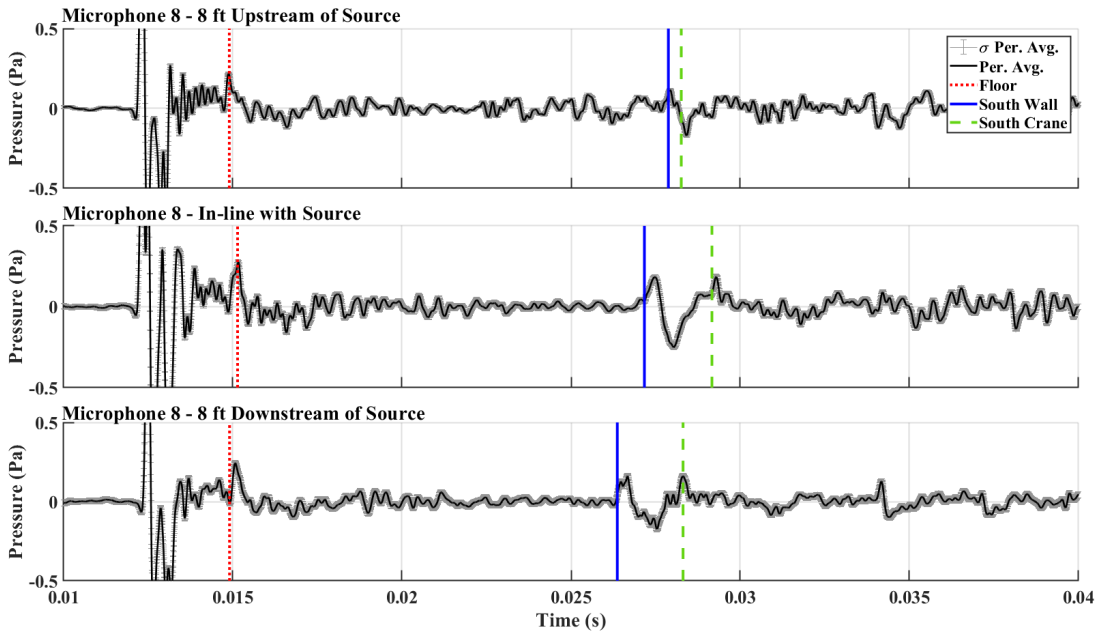

Figure 5: Sensitivity of strong reflections to array streamwise position for microphone 8 with an impulse signal from the dodecahedron.

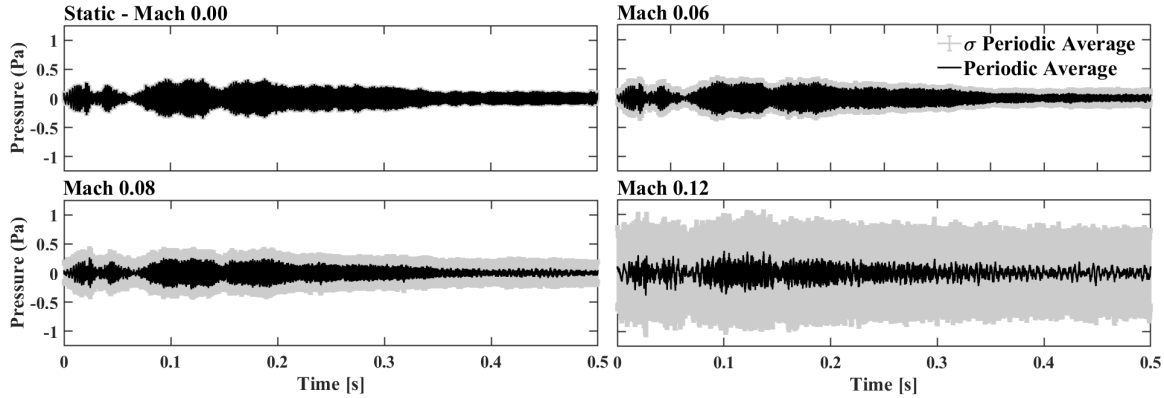

Figure 6: Periodically averaged pressure data for the periodic multisine waveform.

Any good-faith representation of an average should also include a measure of the variability in the data. The standard deviations of the 0.5-second segments for the periodic multisine waveform are included in Figure 6 and provides a useful illustration of one of the difficulties of periodically averaging acoustic pressure data: measuring through a turbulent shear layer. The general shape of the periodically averaged pressure is consistent across the freestream Mach numbers shown in the figure, however the higher Mach number, 0.12, shows the method beginning to struggle to accurately capture the waveform. The variation in the 0.5-second segments is also clear as the magnitude of the standard deviation of the periodically averaged signals increases with increasing Mach number. The effect of the shear layer was even more qualitatively apparent for tones, and in particular, tones with a small wavelength. Figure 7 shows the results of periodically averaging the pressure data at the same Mach numbers for a 300-Hz pure-tone waveform. Note that, although a pure tone is a sine wave with its own period, the periodic averaging for each pure tone was performed over a larger period of 10 ms regardless of the period of the sine wave (three periods of the sine wave for the 300-Hz tone). This

was done to avoid errors that could arise with high-frequency tones where the period of the tone was small enough relative to the sampling frequency such that one period of the sine wave could not be resolved. The interference of the shear layer with the pure sine wave signal led to both amplitude and phase distortions of the waveform at the microphone, increasing the variation across the segments and attenuating the mean amplitude, which can be seen in Figure 7.

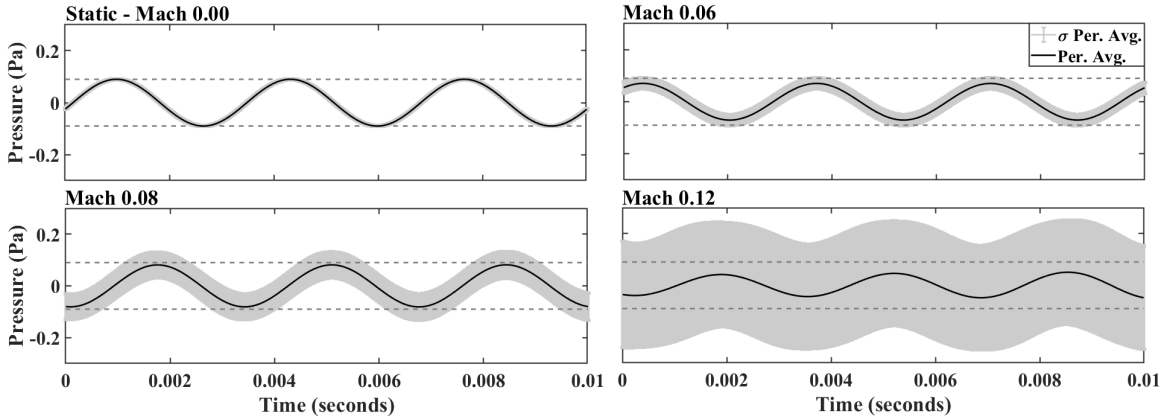

Figure 7: Example of periodic-averaging sensitivity to the shear layer for a pure-tone waveform. The dashed lines in each plot are the boundaries of the periodically averaged waveform in the static condition.

The periodically averaged pressure data from the pure-tone signal indicates that care needs to be taken when applying this method, however, Figure 8 demonstrates the value of periodic averaging when interrogating single-microphone data with a signal-to-noise ratio (SNR) that approaches or falls below 0 dB. The autospectra in Figure 8 were calculated using the periodically averaged pressure data shown in Figure 6. Periodically averaging the data allowed for the isolation of the waveform signal and the rejection of background noise at lower frequencies. At the highest Mach number shown, Mach 0.12, the waveform is still retained even though the background noise levels are up to 20 dB greater than the waveform signal. There are still limitations to periodic averaging, however. The periodically averaged spectra show an attenuation of the higher-frequency content of the waveform for all three Mach numbers. This is especially meaningful since comparing the raw and static autospectra show that the higher-frequency content was captured by the microphone since the SNR was much greater than 30 dB at these frequencies. The attenuation at the high frequencies is likely due to the turbulent shear layer, similar to the distortion effects shown with the pure-tone signal. This suggests that there are limitations to the method of periodic averaging when measuring through a turbulent shear layer, however, most of the periodic content generated by rotorcraft is likely to be at low frequencies, where the attenuation is less severe.

3.3. Low-Frequency Test Section Pressure Wave

A discrepancy in background flow noise was observed during testing between the microphones of the phased array and linear array. As noted in Section 2, the microphones in the linear array were covered with a wind screen, whereas the microphones used in the phased array were not (note that the diaphragms of the phased array microphones were protected with grid caps). The low- to mid-frequency range of the background noise autospectra of the uncovered microphones were upwards of 15 dB greater than the covered microphones at a range of Mach numbers. An

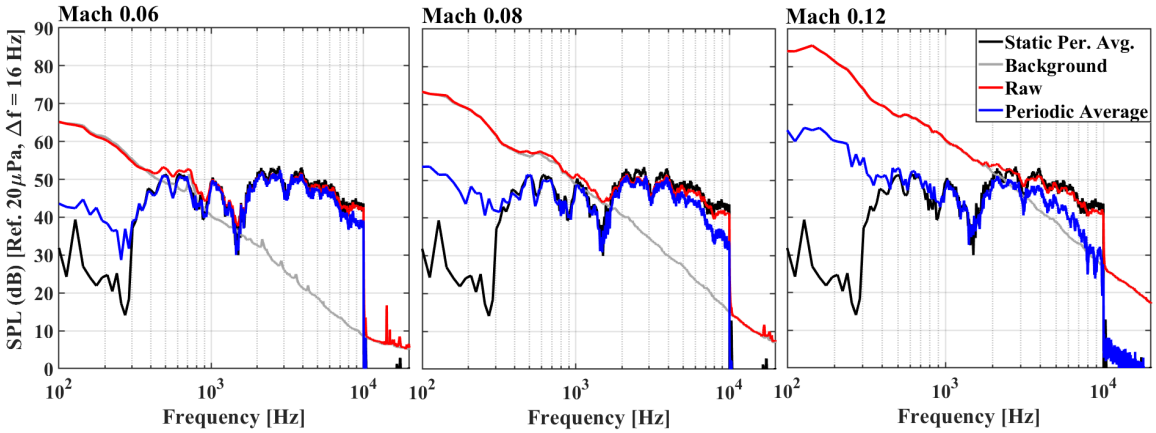

Figure 8: Autospectra of periodically averaged data for the periodic multisine waveform.

investigation of the acoustic data indicated that the uncovered microphones were experiencing an additional hydrodynamic pressure wave that occurs roughly once every 10 seconds. This is the result of a known phenomenon that affects closed-circuit open-jet wind tunnels, where a "low-frequency" (as a description of the frequency of occurance, not the acoustic frequency content) pressure wave moves through the tunnel circuit and passes through the test section [15–17]. It has been determined that these low-frequency pressure fluctuations are worse in a quasi-open-jet with a floor, like in the 14x22, than in a truly open-jet tunnel [18]. This phenomenon has been characterized as a function of test section dynamic pressure and therefore, for an atmospheric tunnel, freestream velocity. During this work, the effect of the low-frequency pressure wave was observed to be the most significant around Mach 0.04 to 0.06. Past efforts have been undertaken in the 14x22 with this phenomenon in mind, however they were focused on test section turbulence and not acoustics [9, 19, 20]. Unfortunately, these efforts largely produced solutions that, while having the desired effect on the low-frequency pressure wave, were strong acoustic sources and therefore are not installed for acoustic tests in the 14x22. Figure 9 shows representative samples of the intermittent pressure spikes caused by the low-frequency pressure pulse with the tunnel flow on but without an acoustic source. The pressure time series data also demonstrate the difficulty of systematically identifying, and therefore removing, this pressure pulse based on the time series data alone. Obvious instances of the pressure pulse are observable, such as around 18 seconds in the Mach 0.02 data set or roughly 33 seconds in the Mach 0.06 data set, however other probable instances are also observably present in the data. This led to a need to identify a systematic way to remove the pressure pulse contamination.

Given that the goals of this work did not include investigating mitigation strategies for this pressure wave, efforts were made to find a systematic method for removing the contamination from the data. This was done by employing a type of averaging that is reminiscent of periodic averaging. The pressure data were again divided into segments at regular time intervals, after which the autospectrum for each interval was calculated. The output of the median averaging method was determined to be insensitive to the widths of the time segments between 0.01 and 1 seconds. The top row of Figure 10 shows the autospectra from 0.51-second intervals (colored lines, roughly 117 distinct autospectra for a 60-second data set). The median of the autospectra is then found for each frequency bin (black line). The time interval of 0.51 seconds was selected to avoid phase locking with the multisine waveform, which had a period of 0.5 seconds. Note that each autospectrum actually contained the frequency content of the first 0.5 seconds of the interval. The last 10 ms of each interval was removed during the conversion to the frequency domain, however, this small deviation between the

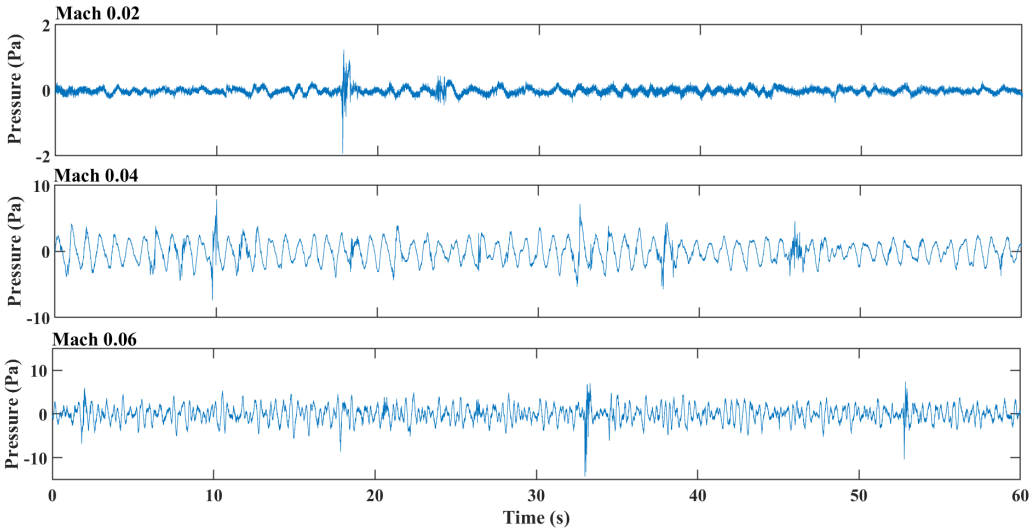

Figure 9: Representative samples of the low-frequency pressure wave in the test section.

period of the waveform and the period of the time interval allowed the resulting median-averaged autospectra to retain the frequency content of the waveform signal and reject the influence of the low-frequency pressure wave. The bottom row of Figure 10 compares the single raw autospectra of the full 60-second data set and the results of the median-averaging method.

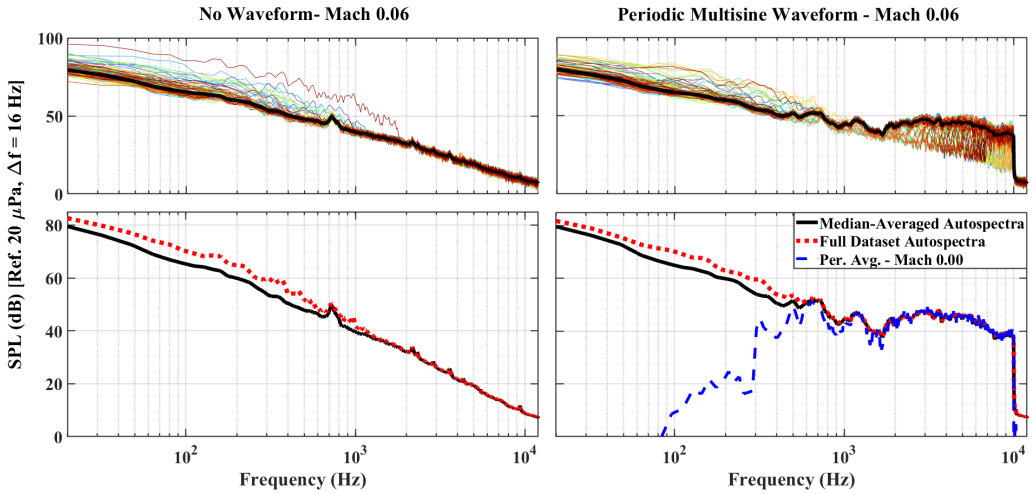

Figure 10: Examples of median averaging, where each unlabeled curve is the autospectrum from a 0.51 second section of the sampled data.

The measured background flow noise levels from the uncovered microphones agreed with the levels measured by the microphones covered by the wind screens after the median-averaging method was applied. This suggested that either the linear array microphones were not experiencing the low-frequency pressure wave for some reason, or that the wind screens could be effectively shielding the microphones from the hydrodynamic pressure wave. Given the asymmetry of the test section, it was posited that the phased array microphones experienced a more severe shear layer than the linear array microphones, so array position in the test section could be a factor. The wind screen was removed from microphone 8 in the linear tower to investigate this, while the wind screens on the rest of the tower remained. Figure 11 compares the data from microphone 8 and its neighbor, microphone

7, when microphone 8 was uncovered. The autospectra show that the data from microphone 8 was affected by the low-frequency pressure at Mach 0.04, and that applying the median-averaging method brought the data from microphone 8 into agreement with its protected neighbor. This suggested that the wind screen was successfully isolating the microphones from hydrodynamic pressure waves. Note that it was stated above that the effects of the pressure wave were observed to be the worst between Mach 0.04 and 0.06, which was true for the microphones in the phased array, however, Figure 11 indicates that there may also be asymmetry effects as well, since the tower array experienced significantly lower effects at Mach 0.06. Figure 11 also shows a portion of the pressure time series for both microphones at Mach 0.04, where the low-frequency pressure pulse is clearly captured by the uncovered microphone but not the microphone with the wind screen.

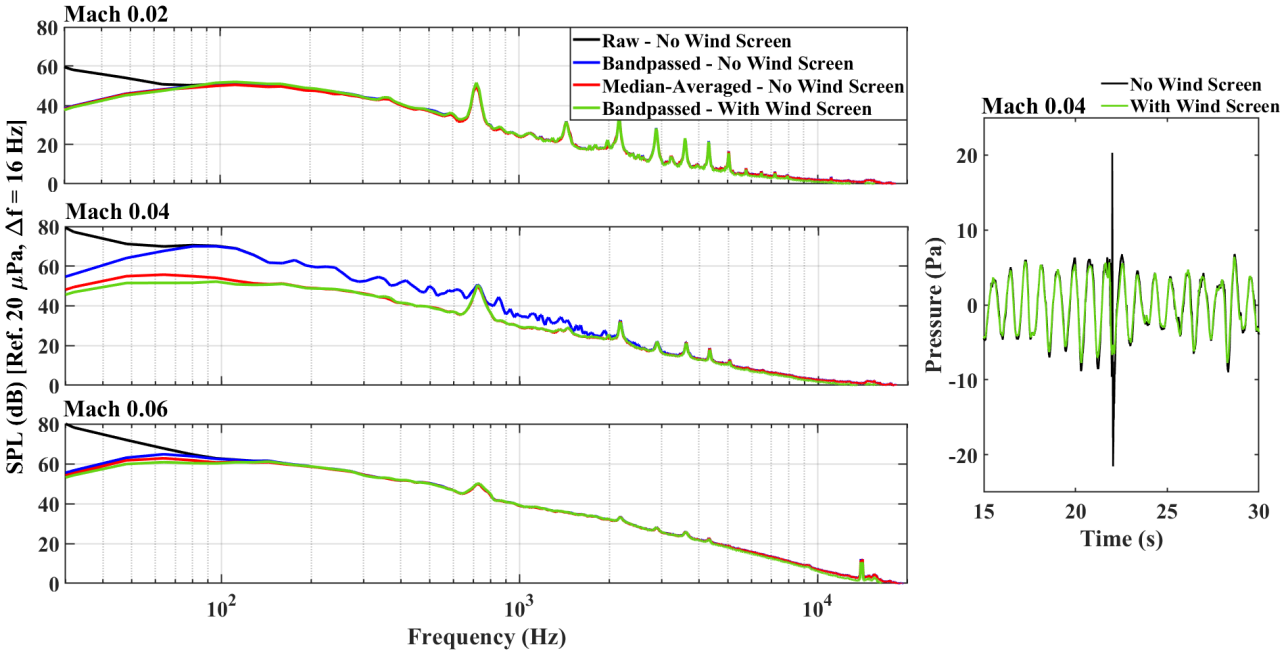

Figure 11: Comparison of raw, median-averaged, and physically-shielded autospectra with the presence of the low-frequency pressure wave (left), and the effect of the wind screen on the recorded pressure signal (right).

There was a concern that the wind screen could be attenuating the high-frequency acoustic content, so the high-frequency broadband random noise source (airball, see Figure 2) was installed while microphone 8 was uncovered to investigate if there was an acoustic penalty to using the wind screens. A comparison of the autospectra from microphones 7 and 8 without tunnel flow indicated less than a 0.5 dB difference below 30 kHz and less than 1 dB difference up to 80 kHz due to the presence of the wind screen. These results suggest that future microphones should be shielded with wind screens for entries in the 14x22.

4. CONCLUSIONS

An acoustic characterization test of the NASA Langley Research Center 14- by 22-Foot Subsonic Tunnel was conducted recently, and this work documents the results from individual microphones in a linear array. A companion paper utilized a phased array during the same test. The goals of

the test were to identify the strongest contributors of reflections in the test section, characterize background flow noise, and to investigate the uses of linear and phased arrays for future rotorcraft tests. The test section floor and walls were identified as strong reflective surfaces, which has informed discussions about additional potential acoustic treatment. Periodically repeating waveforms from known sources helped to investigate the effectiveness of periodic averaging to capture acoustic content for cases with high background flow noise and low signal-to-noise ratios. It was determined that periodic averaging could successfully isolate periodic acoustic signals even when the background flow noise was up to 20 dB greater than the signal. However, high-frequency content was attenuated by periodic averaging, likely due to disruption of the high-frequency content by the turbulent shear layer. Lastly, a processing method for rejecting contamination from a low-frequency hydrodynamic pressure wave in the tunnel circuit was investigated. This median-averaging method was shown to successfully reject the contamination while preserving the background flow noise levels and acoustic source signals. It was also determined that the stretched-nylon wind screens deployed on the linear array microphones were effective at shielding the microphones from the hydrodynamic pressure waves without appreciably affecting the acoustic signal.

ACKNOWLEDGEMENTS

The authors would like to thank the engineers and technicians from LSAWT and the 14x22 for all of their hard work making this test possible, Matthew Galles for his help with designing the new floor treatment, and Nathan Burnside and Clif Horne for providing the airball source. This work was funded by the NASA Revolutionary Vertical Lift Technology (RVLT) project.

REFERENCES

[1] S. L. Heath, T. F. Brooks, F. V. Hutcheson, M. J. Doty, C. J. Bahr, D. Hoad, L. Becker, W. M. Humphreys, C. L. Burley, D. Stead, D. S. Pope, T. B. Spalt, D. H. Kuchta, G. E. Plassman, and J. A. Moen. NASA Hybrid Wing Body Aircraft Aeroacoustic Test Documentation Report. NASA-TM-2016-219185, National Aeronautics and Space Administration, 2016.

[2] M. R. Khorrami, W. M. Humphreys, and D. P. Lockard. An Assessment of Flap and Main Landing Gear Noise Abatement Concepts. In *21st AIAA/CEAS Aeroacoustics Conference*, Dallas, TX, June 2015. doi: 10.2514/6.2015-2987.

[3] F. V. Hutcheson, D. P. Lockard, and D. Stead. On the Alleviation of Background Noise for the High-Lift Common Research Model Aeroacoustic Test. In *28th AIAA/CEAS Aeroacoustics Conference*, Southampton, UK, June 2022. doi: 10.2514/6.2022-2988.

[4] W. M. Humphreys, D. P. Lockard, and C. J. Bahr. Characterization of slat noise radiation from a High-Lift Common Research Model. *AIAA Journal*, 61(10):4556–4578, 2023. doi: 10.2514/1.J062867.

[5] M. A. Marcolini, D. A. Conner, J. T. Brieger, L. E. Becker, and C. D. Smith. Noise Characteristics of a Model Tiltrotor. In *American Helicopter Society's 51st Annual Forum and Technology Display*, Fort Worth, TX, May 1995.

[6] T. B. Spalt, T. F. Brooks, C. J. Bahr, G. E. Plassman, L. E. Becker, and D. J. Stead. Calibrations of the NASA Langley 14- by 22-Foot Subsonic Tunnel in Acoustic Configuration. In *20th AIAA/CEAS Aeroacoustics Conference*, Atlanta, GA, June 2014. doi: 10.2514/6.2014-2344.

[7] N. S. Zawodny, K. A. Pascioni, A. H. Lind, M. B. Galles, C. M. Stutz, and M. L. Houston. Reflectivity Characterization of In-Flow Acoustic Floor Treatment for the NASA Langley 14- by 22-Foot Subsonic Tunnel. Submitted for publication to *53rd International Congress and Exposition on Noise Control Engineering*, Nantes, France, August 2024.

[8] M. L. Houston, C. M. Stutz, N. S. Zawodny, and K. A. Pascioni. Acoustic Characterization of the NASA Langley 14- by 22-Foot Subsonic Tunnel using a Phased Array. Submitted for publication to *Noise-Con 2024*, New Orleans, LA, June 2024.

[9] G. S. Manuel, J. K. Molloy, and P. S. Barna. Effect of Collector Configuration on Test Section Turbulence Levels in an Open-Jet Wind Tunnel. NASA-TM-4333, National Aeronautics and Space Administration, 1992.

[10] M. Schroeder. Synthesis of low-peak-factor signals and binary sequences with low autocorrelation (corresp.). *IEEE Transactions on Information Theory*, 16(1):85–89, 1970. doi: 10.1109/TIT.1970.1054411.

[11] N. S. Zawodny, D. D. Boyd, and C. L. Burley. Acoustic Characterization and Prediction of Representative, Small-Scale Rotary-Wing Unmanned Aircraft System Components. In *Vertical Flight Society's 72nd Annual Forum and Technology Display*, West Palm Beach, FL, May 2016.

[12] N. A. Pettingill, N. S. Zawodny, and C. S. Thurman. Aeroacoustic Testing of UAS-Scale Rotors for a Quadcopter in Hover and Forward Flight. In *28th AIAA/CEAS Aeroacoustics Conference*, Southampton, UK, June 2022.

[13] C. S. Thurman, N. S. Zawodny, and N. A. Pettingill. The Effect of Boundary Layer Character on Stochastic Rotor Blade Vortex Shedding Noise. In *Vertical Flight Society's 78th Annual Forum and Technology Display*, Fort Worth, TX, May 2022.

[14] N. S. Zawodny, N. A. Pettingill, L. V. Lopes, and D. J. Ingraham. Experimental Validation of an Acoustically and Aerodynamically Optimized UAM Proprotor Part 1: Test Setup and Results. NASA-TM-20220015637, National Aeronautics and Space Administration, 2023.

[15] G. Wickern, W. von Heesen, and S. Wallmann. Wind tunnel pulsations and their active suppression. *Journal of Passenger Cars: Mechanical Systems Journal*, 109:1403–1416, 2000. doi: 10.4271/2000-01-0869.

[16] X. Hu, Y. Luo, J. Leng, P. Guo, T. Yu, and J. Wang. The low frequency pressure pulsation and control of the open-jet wind tunnel. *Scientific Reports*, 12:19090, 2022. doi: 10.1038/s41598-022-22080-9.

[17] H. Xingjun, L. Yufei, S. Keyuan, G. Peng, and W. Jingyu. Suppressing methods of the pressure fluctuation in open jet wind tunnels. *Journal of Applied Fluid Mechanics*, 16(10):1901–1915, 2023. doi: 10.47176/jafm.16.10.1889.

[18] L. Jin, X. B. Deng, X. Wang, Y. Gu, Y. Liang, and Z. Lian. Standing waves in the plenum of an open jet wind tunnel: Resonance and self-excited oscillation. *AIP Advances*, 12:025105, 2022. doi: 10.1063/5.0067202.

[19] R. M. Martin, T. F. Brooks, and D. R. Hoad. Reduction of background noise induced by wind tunnel jet exit vanes. *AIAA Journal*, 23(10):1631–1632, 1985. doi: 10.2514/3.9136.

[20] W. L. Sellers, Z. T. Applin, J. K. Molloy, and G. L. Gentry. Effect of Jet Exit Vanes on Flow Pulsations in an Open-Jet Wind Tunnel. NASA-TM-86299, National Aeronautics and Space Administration, 1985.